Transportational cyclic steps created by flow over an erodible bed. Part 1. Experiments.

KAZUO TAKI, *Department of Life and Environmental Science, Chiba Institute of Technology, Tsudanuma 2-17-1, Narashino, Japan 275-8588*
and
GARY PARKER. *St. Anthony Falls Laboratory, University of Minnesota, Minneapolis, MN, USA 55414*

ABSTRACT

Froude-supercritical flow over a flat, erodible bed with copious transport of sediment in suspension appears to be fundamentally unstable. Under a broad range of conditions the flow and bed co-evolve into a series of spatially periodic, or cyclic steps. Each step has a gently sloping Froude-subcritical upstream portion followed by a steeply sloping Froude-supercritical downstream portion, ending in a hydraulic jump which reduces bed shear stress to the threshold value for bed erosion. The steps migrate upstream while preserving form, with net erosion over most of the supercritical region and net deposition over most of the subcritical region. Erosion and deposition balance over one wavelength, so that no average bed erosion results. The successive passage of steps reworks the bed, however, to a depth corresponding to the height of the steps. In the case of silt, the morphology has a strongly step-like character. With fine sand, however, the steps can devolve into the limiting case of chute-and-pool morphology, for which the region of supercritical flow is not so steep.

1. Introduction

The topic of this research is a spatially periodic bedform associated with Froude-supercritical open channel flow over an erodible bed. In particular, if the equilibrium Froude number in the absence of bedforms is sufficiently high, the flow and bed often co-evolve into a series of steps. Each step consists of an upstream portion with Froude-subcritical flow over a bed with a relatively mild (or even adverse) slope and a downstream portion with Froude-supercritical flow over a relatively steep bed. The Froude-supercritical flow terminates in a hydraulic jump at the downstream end. The train of steps migrates slowly upstream.

A series of four such steps can be seen in Fig. 1. The inherent spatial periodicity prompted the authors to name the phenomenon “cyclic steps.” Fig. 2 shows a closer view of two cyclic steps for which the hydraulic jumps are clearly visible. Fig. 3 illustrates the tendency for the steps to migrate upstream while preserving form. It is the goal of the present paper to provide a comprehensive experimental study of cyclic steps. A finite-amplitude theory for their formation is presented in the companion paper, Sun and Parker (submitted)

The present research was motivated by a rather curious event that occurred in the early 1990's. At the time, experiments on alluvial fans were being conducted at St. Anthony Falls Laboratory, University of Minnesota (Whipple et al., 1998). The experimental fans were built up by avulsing channels that were generally braided. The undergraduate research assistant conducting the experiments was John Ahern (as noted in the acknowledgements). Having observed a phenomenon he could not explain, he called the second author over to observe it. A train of four steps, each terminating in a hydraulic jump, had formed in the main channel on the fan. Each step migrated upstream, preserving form, until it reached the apex of the fan and disappeared, only to be replaced by a new step forming from the downstream end.

Cyclic steps represent a generalization of the chute-and-pool morphology discussed in Simons et al. (1965). The description of the morphology therein is, however, rather vague. Fukuoka et al. (1982) provide a comprehensive accounting of bedforms in Froude-supercritical flow, in which upstream-migrating chute-and-pool morphology is more clearly defined. Chute-and-pool morphology is a limiting case of cyclic steps for which the steepest bed slope realized just upstream of the hydraulic jump is still rather mild. Since the present phenomenon encompasses bed slopes that can be so steep that the morphology is truly step-like, the term "cyclic steps" is used here for the entire class of spatially periodic bedforms where each wavelength is delineated by an upstream and downstream hydraulic jump.

Winterwerp et al. (1992) clearly describe a phenomenon that they observed both in the field and laboratory that can be none other than cyclic steps. Their insightful analysis of the phenomenon captures many of the important features of cyclic steps, including the pattern of flow and sediment transport over them. This notwithstanding, it does not explain the steps themselves. More specifically, it falls somewhat short of a complete theory of the maintenance of steps as a stable self-formed finite-amplitude morphology.

At the high Froude numbers characteristic of cyclic steps the dominant mode of transport is typically suspended load. The steps studied here are termed "transportational" because they are associated with spatially varying patterns of erosion of sediment into and deposition from suspension. In particular, deposition dominates on the upstream side of a single step, whereas erosion dominates on the downstream side. While erosion and deposition do not balance at a point, they do balance when averaged over one wavelength, so that the bed profile averaged over steps remains constant in time as sediment is transported through. Purely erosional cyclic steps can occur in the case of flow over a cohesive bed or bedrock. These steps are studied in Parker and Izumi (2000). In such a case the bed shows a constant rate of bed degradation when averaged over the steps.

2. Experimental Setup And Procedure

The flume used in the experiments is shown in Fig. 4. It was constructed of clear, smooth plastic, and had a width of 5 cm. The flume was designed to be narrow in order to suppress three-dimensional effects. The length of the flume was 2 m for most of the experiments, but several experiments were conducted with a length of 4 m in order to better document the spatial periodicity of the steps. Water and sediment were introduced from the upstream end at a constant rate. Both were allowed to escape freely from the downstream end across a low tail weir.

The three types of sediment used in the experiments were relatively well-sorted, commercially available materials that are referred to here as Quartz 19, Silica 45 and Silica 120, the respective characteristic grain sizes D being 19 mμ, 45 mμ and 120 mμ. The material was free of mineral clay. This notwithstanding, all three sizes appeared to exhibit a degree of apparent cohesivity. The material exhibiting the most apparent cohesivity was Silica 45. In all cases the sediment density ρ_s was very close to 2.65

Data acquisition was relatively simple. Bed and water surface elevation could be directly measured from a grid taped to one wall of the flume. The length of the flume was periodically photographed. Data on the bed and water surface profiles were extracted from the photographs by tracing from a projection of the image against a wall. In addition, data on wavelength L, wave height $\Delta\eta$, mean bed slope S_e in the presence of steps and upstream migration speed c defined in Fig. 5 were measured directly from the side wall in the course of the experiments.

In most of the experiments, the bed was initially filled with sediment to the level of the downstream weir, as shown in Fig. 6. Water and sediment were then introduced from the upstream end. Water was delivered from a calibrated constant-head tank, and sediment was delivered from a screw-type feeder; the two were mixed in a funnel before introduction into the flume. The bed then both prograded and aggraded toward an equilibrium bed profile. As described in Fig. 6, this process generally consisted of the downstream translation of a profile with a constant slope. The process of step formation usually did not begin until this profile had propagated either to or nearly to the end of the flume.. Because of this, it was possible in most cases to obtain measurements of the equilibrium slope S_n and depth of the flow h_n over a flat bed in the absence of steps (the "n" denoting "no steps"). An example of this state before step formation is shown in Fig. 7.

Two sets of experiments were conducted. The main set of experiments was conducted in 1994 using a flume length of 2 m, and employing all three types of sediment. In many of these experiments, however, only a single step would form in the flume due to its shortness. The cyclicity of the phenomenon was verified by the repeated formation of a new step at the downstream end of the flume as or after the previous one reached the upstream end and vanished. An auxiliary set was conducted in 1997 using only the Silica 45 material. For three of the seven experiments in this set the flume length was extended to 4 m in order to more clearly

verify the spatial periodicity of the phenomenon. Fig. 1 is an image from one of these experiments.

3. Experimental Results

The basic data taken in the course of the experiments of 1994 are summarized in Table 1. Of interest at this point is the column denoted "Bed Type". Five classifications are given there. They are defined as follows.

- F: flat bed (14 experiments). In these cases bedforms never evolved. There could be at least three reasons for this. The flow may not have been in the range for cyclic step formation, the equilibrium wavelength of the steps may have been too long to be expressed in a flume with a length of 2 m, or not enough time may have been allowed for development.
- SS: single step (13 experiments). In these cases only a single upstream-migrating step was observed. Either slightly before or sometime after the step had migrated into the upstream end of the flume and disappeared, a new step would appear at the downstream end. In such cases the flume was too short to contain multiple steps and so step wavelength could not be measured.
- CS: cyclic steps (22 experiments). In these cases two or more upstream-migrating steps were observed simultaneously, allowing for a determination of step wavelength.
- SCP: steps having the character of chute-and-pool morphology (2 experiments). These upstream-migrating steps had maximum bed angles that were quite low.
- DMSH: downstream-migrating scour holes (5 experiments). These curious features appear not to have been recognized elsewhere in the literature. They are discussed separately below. In some cases upstream-migrating cyclic steps appeared in runs that also exhibited downstream-migrating scour holes.

Fig. 8 illustrates the formation of cyclic steps in the Quartz 19 material. Figs. 1 and 2 illustrate cyclic steps formed in the Silica 45 and Silica 120 material, respectively. The following can be discerned between the three images: a) the spatial periodicity of the phenomenon, b) the presence of a hydraulic jump at the downstream end of each step, c) the tendency for the bed to be steepest just upstream of the hydraulic jump and d) the reworking of the bed as the pattern migrates upstream, a feature that is evident due to the incorporation of dyed water in the reworked sediment visible in Fig. 8. The predominant mode of sediment transport was observed to be suspension. Even with the narrow width of 5 cm, flow occasionally concentrated to one side or the other of each step, introducing an element of flow meandering. Here, however, the study is focused on one-dimensional steps for which the tendency to meander was small.

The basic data in Table 1 consists of the following parameters; volume water discharge Q_w, mass sediment feed rate G_s, volume sediment feed concentration χ_f given by the relation

$$\chi_f = \frac{(G_s/\rho_s)}{Q_w + (G_s/\rho_s)} \tag{1}$$

where ρ_s denotes sediment density, depth h_n measured while the bed was still flat, slope S_n measured while the bed was still flat, upstream step migration speed c, step height $\Delta\eta$ and step wavelength L. Here step height is defined as the maximum normal deviation from the straight line connecting the bottom of one pool at a hydraulic jump to the bottom of the next pool downstream, as defined in Fig. 5.

The data given in Table 1 are subject to the following estimates of experimental error. Water discharge Q_w and sediment feed rate G_s was determined within $\pm$ 4 percent and $\pm$ 10 percent, respectively. All length measurements were accurate within about 1 ~ 2 mm with the exception of depth h_n. Even though special care was taken to measure depth as accurately as possible, the measurements may be in error by as much as 0.5 mm. Because depth h_n itself is on the order of only a few mm, the implication is that the values for that parameter are the least accurate of Table 1. Measurements of time of upstream migration for determining upstream migration rates were accurate to within a few seconds. It should be understood, however, that additional error enters into the numbers because the number of steps over which parameters were averaged was typically less than four.

In Table 1, the values for depth h_n, vary from 1.2 mm to 7.0 mm. Bed slope S_n varies from 0.0185 to 0.166, falling at the very high end of those observed in equilibrium mobile-bed open channel flows. The concentration of sediment in the feed χ_f is also high, varying from 0.0034 to 0.22. In 34 of the 51 experiments, however, χ_f is less than 0.05, indicating that the feed suspension was dilute in most cases. Upstream step migration speed varies from a low of 0.02 cm/s to a high of 0.90 cm/s. Step height $\Delta\eta$ varies from 1.9 to 6.6 cm and step wavelength L varied from 55 cm to 130 cm. The measurement of longer step lengths was prohibited by the flume length of 2 m.

Both the cyclic steps obtained in the present study and the flow over them strongly satisfy the slender-flow approximation, i.e. that the characteristic scale of change in the streamwise direction (step wavelength in this case) should be many times the characteristic scale of change in the upward normal direction (flow depth in this case). That is, the ratio L/h_n was found to typically be in the range 100 – 500. It is under this condition that the Reynolds-averaged Navier-Stokes equations and equations of mass conservation can be reduced to the depth-averaged de St. Venant equations shallow-water equations (e.g. Graf and Altinakar, 1993). With this in mind, it should be possible to explain the formation and maintenance of cyclic steps in the context of the shallow-water equations. Such a treatment is pursued in the companion paper, Sun and Parker (submitted).

4. Relations for resistance and sediment entrainment

As noted above, the predominant mode of sediment transport appeared to be suspension. Of primary importance to the theory of the companion paper, Sun and Parker (submitted) are the determination of empirical relations for bed resistance and sediment entrainment appropriate to a flow over a flat bed without steps. The data of Table 1 allow for the approximate determination of such a relation.

Even though the flows are very thin, the relatively narrow width of the flume of 5 cm dictates that the effect of the sidewalls must be removed before seeking such relations. Here this is done using the procedure outlined in Vanoni and Brooks (1957) for rectangular channels with smooth walls. Bed and wall friction coefficients C_{fb} and C_{fw} are defined as follows;

$$\tau_b = \rho C_{fb} u_{nb}^2 , \quad \tau_w = \rho C_{fw} u_{nw}^2 \tag{2a,b}$$

where u_{nb} and u_{nw} denote the mean flow velocities of the bed and wall regions in the absence of steps, τ_b and τ_w denote the associated mean boundary shear stresses of the bed and wall regions and ρ denotes the density of water. Under the conditions of the equilibrium flow attained before the development of steps, the following forms for momentum balance hold;

$$\tau_b = \rho g r_b S_n , \quad \tau_w = \rho g r_w S_n \tag{3a,b}$$

where g denotes the acceleration of gravity and r_b and r_w are given by the relations

$$r_b = h_n (1 - \frac{h_n}{B}), \quad r_w = \frac{h_n}{2} \tag{4a,b}$$

where B denotes flume width.

The following relation was adopted for the computation of C_{fw};

$$C_{fw} = \begin{cases} 0.03952\, \mathbf{Re}_w^{-0.25} & \text{for} \quad \mathbf{Re}_w \geq 2000 \quad (\text{turbulent flow}) \\ 64\, \mathbf{Re}_w^{-1} & \text{for} \quad \mathbf{Re}_w < 2000 \quad (\text{laminar flow}) \end{cases} \tag{5}$$

where $\mathbf{Re}_w$ denotes a wall Reynolds number equivalent to pipe flow given by the relation

$$\mathbf{Re}_w = \frac{4 r_w u_{nw}}{\nu} \tag{6}$$

in which ν denotes the viscosity of the fluid, here approximated by the viscosity of clear water (e.g. Chiew and Parker, 1994).

The removal of wall effects allow a determination of the flow velocity of the bed region u_{nb}, the bed friction coefficient C_{fb}, the Reynolds number of the bed region $\mathbf{Re}_b$ and the Shields stress of the bed region τ_b^*, the latter two parameters being given by the relations

$$\mathbf{Re}_b = \frac{4 r_b u_{nb}}{\nu}, \quad \tau_b^* = \frac{\tau_b}{\rho R g D} \tag{7a,b}$$

where D denotes grain size and

$$R = \frac{\rho_s}{\rho} - 1 \tag{8}$$

denotes the submerged specific gravity of the sediment. The computed values of $\mathbf{Re}_b$, τ_b^* and C_{fb} for the 1994 runs under flat-bed conditions are given in Table 2.

Of the 45 runs listed in Table 2, it is seen that 31 have values of $\mathbf{Re}_b$ in excess of 2000, and 14 have values below 2000. The implication is that in some of the runs the flow may have been laminar in the absence of steps. In the presence of steps, however, the existence of a hydraulic jumps ensures the generation of considerable turbulence. Since the case of interest here is turbulent flow carrying suspended sediment, only data clearly pertaining to turbulent flow were used to describe bed resistance and sediment entrainment.

Of the various ways to describe bed resistance, the best results were obtained from a plot of C_{fb} versus relative roughness h_n/D. The results are shown in Fig. 9. Although the data show considerable scatter there is no obvious trend, with a typical value of C_{fb} near 0.01. The individual values of C_{fb} were averaged to yield three characteristic values C_{fa}, one for each sediment type studied. These values are listed in Table 3 along with grain size D, particle Reynolds number $\mathbf{Re}_p$ given by the relation

$$\mathbf{Re}_p = \frac{\sqrt{RgD}\,D}{\nu} \tag{9}$$

and particle fall velocity v_s determined from the Dietrich (1982) relation. In (9) ν denotes the kinematic velocity of the fluid: this value has been approximated using the clear-water value at 20° C.

Observation of the hydraulic jumps indicated that the bed shear stress was reduced to the threshold value for bed erosion immediately behind the jump. With this in mind, the Froude number $\mathbf{Fr}_t$ and threshold velocity u_t on the downstream side of the jump was determined from measurements of flow depths h_u just upstream of the jump and h_d just downstream of the jump and the standard relation for conjugate depth;

$$\frac{h_u}{h_d} = \left(\frac{\sqrt{1+8\mathbf{Fr}_t^2}-1}{2} \right)^{-1} \tag{10}$$

where

$$\mathbf{Fr}_t^2 = \frac{u_t^3}{gq_T}, \quad q_T = \frac{Q_w + (G_s/\rho_s)}{B} \tag{11}$$

In the above relations q_T denotes the total volume discharge per unit channel width.

Data from seven hydraulic jumps for the experiments in the Quartz 19 material (Runs 26 and 26), four hydraulic jumps for the experiments in the Silica 45 material (Run 6) and nine hydraulic jumps for the experiments in the Silica 120 material (Runs 7 and 9) were used in conjunction with the above relations to estimate values of u_t for each sediment size. The values so determined, which are on the order of 10 cm/s, are listed in Table 3. Estimates of the critical or threshold

Shields stress τ_{th}^* for the erosion of bed sediment were determined for each sediment size from the following relation;

$$\tau_{th}^* = \frac{C_{fa} u_t^2}{R g D} \tag{12}$$

These values are also listed in Table 3.

Mantz (1977) has offered a relation for the threshold Shields stress for fine material that can be cast in the following form;

$$\tau_{th}^* = [0.1(\mathbf{Re}_p)^{-0.3}]^{(1/1.15)} \tag{13}$$

In Fig. 10 the values of τ_{th}^* of Table 3 are compared with those predicted by (13). In the case of the 120 mμ and 45 mμ material the agreement between the two is nearly perfect. In the case of the 19 mμ material the experimentally determined value is about twice the predicted value. In light of the excellent agreement in the case of the 120 mμ and 45 mμ material, it is concluded that the hydraulic jump does indeed act to reduce the bed shear stress to the value associated with the threshold of erosion. The disagreement in the case of the 19 mμ material is likely due to the fact that it is extremely fine, and thus subject to apparent cohesivity that cannot be easily predicted from parameters related to fluid mechanics alone.

The depth-averaged equation of mass balance of suspended sediment can be written in the following form;

$$\frac{\partial \chi h}{\partial t} + \frac{\partial q_s}{\partial x} = v_s (E - r_o \chi) \tag{14}$$

where χ denotes local depth-averaged volume sediment concentration, h denotes local flow depth, q_s denotes the local volume transport rate of suspended sediment per unit width, E denotes the dimensionless rate of entrainment of sediment into suspension from the bed and r_o is a shape factor relating near-bed sediment concentration to depth-averaged sediment concentration. The parameter E is generally related to bed shear stress and other parameters (e.g. Garcia and Parker, 1991).

Under the conditions of the flat-bed equilibrium state prevailing before the formation of steps, (14) reduces to

$$E = r_o \chi \tag{15}$$

In the case of the present experiments the flows were so thin that it was impossible to determine a vertical distribution of suspended sediment. In addition, the opacity of the flow appeared to be relatively uniform in the vertical direction. Here it is assumed that the near-bed volume sediment concentration $r_o\chi$ is equal to the vertically averaged value χ, so that r_o is approximated as unity. As a result, E is approximated as χ for the case of flat-bed equilibrium. The data of Tables 1 and

2 pertaining to verifiably turbulent flow ($\mathbf{Re}_b$ > 2000) were thus used to determine a relation for sediment entrainment into suspension of the following form;

$$E = \alpha_t [\tau_b^* - \tau_{th}^*]^n \tag{16}$$

where the coefficient α_t is assumed to be a function of particle Reynolds number $\mathbf{Re}_p$. This form was modeled after the entrainment relation of van Rijn (1984), which provides good predictions for flows with larger values of the ratio h/D. The exponent n was set equal to the value 1.5 recommended by van Rijn as well as the values 1.8 and 2.0, and the coefficients α_t were fitted to the data. The coefficients α_t are given in Table 3. In Fig. 10 the values of α_t so determined are plotted as a function of $\mathbf{Re}_p$. In Figs. 11a,b,c values E/α_t predicted by (16) are compared against the data for the three cases of n. While the plots show considerable scatter, the data from the three sets do collapse together to define a sensible relation for sediment entrainment. It does not seem possible, however to say that any one of the choices of n is clearly superior to any of the other two.

It is reasonable to assume that the relations obtained above for resistance and sediment entrainment when steps are absent also apply locally in the case for which steps are present. This is particularly true in light of the fact that the steps and the flow over them satisfy the slender-flow approximation very well. With this in mind, they are used in the companion paper, Sun and Parker (submitted) in order to develop a predictive theory for transportational steps.

5. Analysis of step characteristics

As an introduction to a study of step characteristics, it is of value to introduce three new dimensionless parameters. The first of these is the Froude number $\mathbf{Fr}_n$ of steady, uniform (normal) flow prevailing over a flat bed without steps and with total volume discharge per unit width q_T. It can be defined as follows;

$$\mathbf{Fr}_n^2 = \frac{u_n^2}{g h_n} \tag{17}$$

where u_n is the mean flow velocity in the absence of steps, and u_n and h_n are related by the equation of flow continuity:

$$q_T = u_n h_n \tag{18}$$

Between (17) and (18) it is found that

$$\mathbf{Fr}_n^2 = \frac{q_T^2}{g h_n^3} \tag{19}$$

The second of these is the Froude number $\mathbf{Fr}_t$ associated with the threshold of motion for the specified total volume discharge per unit width q_T. This is estimated here by considering steady, uniform (normal) flow over a bed at the threshold of motion. The associated equations of momentum and mass balance can be written as

$$C_{fa}u_t^2 = gh_tS_t\ , \quad q_T = u_th_t \tag{20a,b}$$

where h_t and u_t denote the flow depth and velocity at the threshold of motion and S_t, the third new dimensionless parameter, is an estimate of the bed slope at the threshold of motion. In (20a) the bed friction coefficient C_{fb} has been approximated with the average value C_{fa} for a given sediment size. Defining $\mathbf{Fr}_t$ as

$$\mathbf{Fr}_t^2 = \frac{u_t^2}{gh_t} \tag{21}$$

and reducing with (20a,b) it is found that

$$\mathbf{Fr}_t^2 = \frac{u_t^3}{gq_T}, \quad S_t = C_{fa}\mathbf{Fr}_t^2 \tag{22a,b}$$

All the information necessary for the computation of $\mathbf{Fr}_n$, $\mathbf{Fr}_t$ and S_t can be found in Tables 1 and 3. Computed values for cases for which steps were observed are listed in Table 4.

In light of the above discussion, step wavelength L, step height $\Delta\eta$ and upstream step migration velocity c might be thought to be functions of the following parameters; g, v_s, u_t, q_t, h_n, S_t and χ_f. A simple dimensional analysis yields the following results. The dimensionless parameters

$$\Delta\hat{\eta} = \frac{u_t}{q_T}\Delta\eta, \quad \tilde{L} = \frac{u_t}{q_T}L, \quad \tilde{c} = \frac{c}{u_t} \tag{23a,b,c}$$

should at most be functions of $\mathbf{Fr}_t$, $\mathbf{Fr}_n$, S_t, ω and χ_f, where

$$\omega = \frac{v_s}{u_t} \tag{24}$$

Values for ω are listed in Table 3 for each sediment size used in the experiments. In fact it can be shown that one of the above five parameters can be eliminated through the use of the entrainment relation. For example, if the first four parameters are specified, the fifth can be computed from the approximation $E \cong \chi$ and (16).

As shown in the companion paper, Sun and Parker (submitted), the parameters can under appropriate conditions be collapsed even further. Let λ_p be the dimensionless parameter denoting the porosity of the bed. Absorbing S_t and χ_f into the dimensionless dependent variables for wavelength and wave speed as follows,

$$\hat{L} = S_t\tilde{L} = S_t\frac{u_t}{q_T}L, \quad \hat{c} = \frac{(1-\lambda_p)}{\chi_f}\tilde{c} = \frac{(1-\lambda_p)}{u_t\chi_f}c \tag{25a,b}$$

it can be shown that the following general forms result;

$$\hat{\lambda} = f_\lambda(\mathbf{Fr}_t, \mathbf{Fr}_n, \omega) \tag{26a}$$

$$\Delta\hat{\eta} = f_\Delta(\mathbf{Fr}_t, \mathbf{Fr}_n, \omega) \tag{26b}$$

$$\hat{c} = f_c(\mathbf{Fr}_t, \mathbf{Fr}_n, \omega) \qquad (26c)$$

As a first step toward characterizing step formation, bed type is plotted as a function of $\mathbf{Fr}_n$ and $\mathbf{Fr}_t$ for each sediment type (i.e. each value of ω) in Figs. 12a-c. The bed types are those given above: F = flat, SS = single step, MS = multiple steps, SCP = steps having the character of chute-and-pool morphology and DMSH = downstream migrating scour holes.

The first point of interest is that all the values of $\mathbf{Fr}_t$ pertaining to steps (single or multiple) are between 0.2 and 0.8. The second point of interest is that all the values of $\mathbf{Fr}_n$ pertaining to steps are between 1 and 3.5, with the exception of two cases for the 45 micron material for which $\mathbf{Fr}_n$ takes the values 0.65 and 0.84. Thus with only minor exception the data suggest that the regime for the formation of cyclic steps is one for which $\mathbf{Fr}_n > 1$ and $\mathbf{Fr}_t < 1$.

The implication is that at least a large subset of the regime $\mathbf{Fr}_n \in (1, \infty)$, $\mathbf{Fr}_t \in (0, 1)$ has the character that the equilibrium Froude-supercritical normal flow in the absence of steps is fundamentally unstable. Stability is achieved only when the flow devolves into a series of steps, each terminating in a hydraulic jump that locally reduces Froude-supercritical flow to a Froude-subcritical state at the threshold of motion.

Fig. 12a for the 19 micron material contains the largest number of data points. The range for multiple steps appears to be such that $\mathbf{Fr}_t \leq 0.4$. The likely conclusion is that step wavelength increases with increasing $\mathbf{Fr}_t$, such that for sufficiently large values only a single step would form in the 2-m long flume used in the experiments. The same conclusion can be drawn for the 45 micron material of Fig. 12b and the 120 micron material of 14c.

Fig. 12c suggests that in the limit as $\mathbf{Fr}_t$ approaches unity the bed becomes flat. In Figs. 12a and 12b, however, there are several points associated with a flat bed that are interspersed within the regime for which steps are observed. In these cases not enough time may have been allowed for the formation of steps in the execution of the experiments.

Fig. 12c shows another interesting feature. In the case of the two largest values of $\mathbf{Fr}_t$ for which steps are observed, the steps have the character of chute-and-pool morphology. That is, the downstream end of the supercritical regime does not show the strong step-like character of the other experiments. The implication is that a truly step-like character may become more difficult to obtain as the bed sediment becomes coarser than about 100 microns, so that the limiting case of chute-and-pool topography is realized instead.

The downstream-migrating scour holes of Figs 12a,b are discussed separately below.

The data for dimensionless wave speed $\hat{c}$, wave height $\Delta\hat{\eta}$ and wavelength $\hat{L}$ are plotted against $\mathbf{Fr}_t$ and $\mathbf{Fr}_n$ for the 19 micron and 45 micron materials in Figures 13a,b, 14a,b and 15a,b. (Data for the 120 micron material are insufficient.) Wave speed $\hat{c}$ decreases and wave height

$\Delta\hat{\eta}$ and wavelength $\hat{L}$ increase strongly as $\mathbf{Fr}_t$ increases. The variation in $\mathbf{Fr}_n$ is less strong, but wavelength $\hat{L}$ appears to increase mildly as $\mathbf{Fr}_n$ increases.

The data in Tables 1 – 4 pertain to the 1994 experiments, and were obtained by means of observations taken directly from the side walls of the flume. Some data, however, were extracted from photographs taken of the 1994 and 1997 experiments. The data obtained in this way are listed in Table 5. The error ranges in the measurements of Table 5 are similar to those quoted above for Table 1. Some of the values in Table 5 differ somewhat from the data for the corresponding experiment in Table 1 because they pertain to the same experiment at different times. The parameters h_e and S_e listed for some of the experiments in the table correspond to mean depth and bed slope at the global (but not local) equilibrium state associated with the presence of steps. The parameter θ_{max} corresponds to the maximum bed slope angle observed in the region of supercritical flow just upstream of the hydraulic jump. The two values listed for each experiments correspond to the lowest and highest values of θ_{max} measured upstream of three to five jumps for each experiment. The step-like character of the morphology is underlined by maximum bed slopes as high as 15 – 47° just before the hydraulic jump.

6. Downstream-Migrating Scour Holes

A curious morphology that appears not to have been reported upon elsewhere was observed in several of the experiments. This morphology consisted of downstream-migrating scour holes, i.e. the bed type DMSH of Figs. 12a and 12b. Such a scour hole is shown in Fig. 16. The scour hole was observed to contain a recirculating flow that was directed downstream in the upper part of the hole and upstream along the bed of the hole. The result was erosion of the downstream wall of the hole, with the deposition of the material so eroded on the upstream side, so that the hole migrated downstream.

Downstream-migrating scour holes appeared to be transient features associated with minor discontinuities in bed slope. As can be seen from Figs. 12a and 12b, the regime of formation appears to be $\mathbf{Fr}_t < 0.3$ and $\mathbf{Fr}_n < 2$. In some cases cyclic steps appeared after the scour holes had migrated out of the flume. It thus appears that the regimes for the formation of transient downstream-migrating scour holes and cyclic steps of permanent form overlap.

7. Discussion

The transportational cyclic steps described above are not merely an artifact of small-scale experiments. They have been observed in the field by Winterwerp et al. (1992). In particular, cyclic steps in alluvium were observed to form readily under conditions of supercritical flow over fine sand as water flows out of a levee breach in the process of being closed. Such cyclic steps probably also form readily in rivers when the appropriate conditions are met. These conditions are a) a plethora of easily-suspendable sediment such as fine sand and b) slopes and discharges

suitable for the formation of strongly supercritical flow. In most alluvial rivers the sediment transport capacity of supercritical flow is so high that the sediment supply is not sufficient to maintain it in equilibrium. A notable exception, however, is likely to be sandy alluvial fans in a desert environment.

Supercritical flow is also common during floods in steep bedrock streams. These streams are bedrock streams precisely because the sediment transport capacity at flood flow is in excess of the sediment supply. Erosional cyclic steps are commonly observed in such streams (Parker and Izumi, 2000). They are close relatives of the transportational cyclic steps described here.

The case of transportational cyclic steps, i.e. steps of alluvial material that migrate upstream with no mean change in bed elevation, is analyzed in detail here. It should be noted, however, that trains of upstream-migrating steps in alluvium were also observed under conditions of both net bed aggradation and net bed degradation.

It is possible that the experimental steps reported here were partially influence by surface tension. Surface tension is not, however, necessary for their formation, as Winterwerp et al. (1992) have observed them at field scale under conditions for which surface tension can be neglected.

8. Conclusions

Froude-supercritical flow over an erodible bed composed of fine material, for which the dominant mode of sediment transport is suspension, appears to be inherently unstable. Under a wide range of conditions for which the Froude number $\mathbf{Fr}_n$ prevailing in the absence of steps is supercritical and the Froude number $\mathbf{Fr}_t$ associated with the threshold of motion is subcritical, the bed devolves into a series of spatially periodic steps. Each step consists of an upstream zone with a gentle (sometimes adverse) slope and subcritical flow, and a downstream zone with a steep slope and supercritical flow, ending in a hydraulic jump.

These transportational cyclic steps migrate upstream at approximately constant speed while preserving form. They are maintained by a combination of spatially varying erosion and deposition of suspended sediment. The erosion and deposition rates differ from each other from point to point, but balance when averaged over one wavelength. As a result, although the bed is reworked to a depth corresponding to the wave height by passing steps, average bed height remains constant in time. It can be concluded that such steps represent a finite-amplitude equilibrium state of permanent form.

Cyclic steps appear to be self-adjusting so that the boundary shear stress in the hydraulic jumps is reduced to the critical value associated with the threshold of bed erosion. They include chute-and-pool morphology, for which the step-like character of the bedforms is subdued, as a limiting case. This limiting case appears to be realized more easily in relatively coarse bed sediment (i.e. in excess of 100 microns).

An analysis of the data yields relations pertaining to bed resistance and entrainment into sediment for the case of a flat bed in the absence of steps. Because both the cyclic steps observed here and the flow over them are long-wave phenomena (h/L <<1), it is reasonable to assume that the same relations would hold locally in the presence of steps as well. This concept is used in the companion paper, Sun and Parker (submitted), to develop a general theory of transportational cyclic steps.

A range of conditions exists for which downstream-migrating scour holes are observed as a transient morphology. Their formation appears to be associated with lsupercritical values of $\mathbf{Fr}_n$, less than about 2, low subcritical values of $\mathbf{Fr}_t$ and fine sediment.

This research was funded by the U.S. National Science Foundation (CTS-9207882 and CTS-9424507). Thanks are extended to John Ahern for recognizing cyclic steps in the course of experiments on alluvial fans. John Gulliver is also thanks for providing the second author with a leave of absence, during which time this paper was finalized with the first author in Japan. Syunsuke Ikeda kindly provided office space, facilities, and copious discussion time at the Tokyo Institute of Technology. This paper is a contribution of the National Center for Earth Surface Dynamics, a Science and Technology Center funded by the U.S. National Science Foundation. It specifically addresses the Center's research efforts on channel dynamics.

Notations

B	channel width
c, $\tilde{c}$, $\hat{c}$	upstream migration speed; dimensionless upstream migration speed defined by (23c); dimensionless upstream migration speed defined by (25c)
C_{fw}, C_{fb}, C_{fa}	wall friction coefficient; bed friction coefficient; average bed friction coefficient
D	grain size
E	dimensionless rate of entrainment of bed sediment into suspension
$\mathbf{Fr}_n$	Froude number associated with normal flow before the development of steps
$\mathbf{Fr}_t$	Froude number associated with the threshold for bed erosion
g	acceleration of gravity
G_s	mass sediment feed rate
h, h_e, h_n, h_u, h_d, h_t	flow depth normal to bed; mean depth in the presence of steps; depth for a flat bed with no steps; depth just upstream of a hydraulic jump, depth just downstream of a hydraulic jump; depth at threshold for bed erosion
q_s	volume sediment discharge per unit width
q_T	total volume discharge (water + sediment) per unit width

L, $\tilde{L}$, $\hat{L}$	step wavelength; dimensionless step wavelength defined by (23a); dimensionless step length defined by (25b)
Q_T	total volume discharge at feed point (water plus sediment)
Q_w	volume water discharge
q_w	volume water discharge per unit width
r_b	hydraulic radius of bed region
r_w	hydraulic radius of wall region
r_o	dimensionless coefficient in (14)
R	submerged specific gravity of sediment; = (ρ_s/ρ)-1
$\mathbf{Re}_b$	Flow Reynolds number associated with bed region
$\mathbf{Re}_p$	Particle Reynolds number defined by (9)
$\mathbf{Re}_w$	Flow Reynolds number associated with wall region
S_e	mean bed slope in the presence of steps
S_n	bed slope in the absence of steps
S_t	bed slope at the threshold of bed erosion
S_s	mean bed slope in the presence of steps
u_n	mean flow velocity in the absence of steps
u_{nb}	mean flow velocity in bed region in the absence of steps
u_{nw}	mean flow velocity in wall region in the absence of steps
u_t	mean flow velocity at the threshold for bed erosion
v_s	fall velocity of sediment in quiescent water
x	streamwise coordinate
t	time
α_t	coefficient in relation (16) for the entrainment of sediment into suspension
χ, χ_f	volume concentration of sediment in suspension; volume concentration of sediment in feed
$\Delta\eta$, $\Delta\hat{\eta}$	step height; dimensionless step height defined by (23a)
λ_p	bed porosity
ν	viscosity of water
θ_{max}	maximum bed angle of step
ρ	density of water
ρ_s	material density of sediment
τ_b	boundary shear stress on bed region
τ_w	boundary shear stress on wall region
τ_b^*	dimensionless bed Shields stress

τ_{th}^* dimensionless Shields stress at the threshold of erosion

References

DIETRICH, W. E. (1982) Settling velocity of natural particles. *Water Resources Research*, 18(6), 1615-1626.

FUKUOKA, S., OKUTSU, K. and YAMASAKA, M. (1982) Dynamic and kinematic features of sand waves in upper regime. *Proc. Japan Soc. Civil Engrg.,* 323, 77-89.

CHIEW, Y. M. and PARKER, G. (1994) Incipient motion on non-horizontal slopes. *J. Hydr. Res.*, 32(5), 647-660.

GARCIA, M. and PARKER, G. (1991) Entrainment of bed sediment into suspension. *J. Hydr. Engrg.,* ASCE, 117(4), 414-435.

GRAF, W. H AND ALTINAKAR, M. S. (1993). *Hydraulique Fluvial.* Presses polytechniques et universitaires romandes, 259 p.

MANTZ, P. A. (1977) Incipient transport of fine grains and flakes by fluids – extended Shields diagram. *J. Hydr. Engrg.*, ASCE. 103(6), 601-615.

PARKER, G. and IZUMI, N. (2000) Purely erosional cyclic and solitary steps created by flow over a cohesive bed. *J. Fluid Mech.*, in press.

van RIJN, L. C. (1984) Sediment transport. II. Suspended load transport. *J. Hydr. Engrg*, ASCE, 110(11), 1431-1456.

SIMONS, D. B., RICHARDSON, E. V. and NORDIN, C. F. (1965) Sedimentary Structures Generated by Flow in Alluvial Channels. *Special Pub. No. 12*, Am. Assoc. Petrol. Geologists.

SUN, T. and PARKER, G. (submitted) Transportational cyclic steps created by flow over an erodible bed. Part 2. Theory and numerical simulation. *J. Hydr. Res*.

VANONI, V.A. and BROOKS, N. H. (1957) Laboratory studies of the roughness and suspended load of streams. *Rept.* E68, California Institute of Technology, Pasadena, Calif. USA.

WHIPPLE, K. X, PARKER, G., PAOLA, C. and MOHRIG, D. (1998) Channel dynamics, sediment transport and the slope of alluvial fans: Experimental Study. *J. Geology,* 106, 677-693.

WINTERWERP, J. C., BAKKER, W. T., MASTBERGEN, D. R., and VAN ROSSUM, H. (1992) Hyperconcentrated sand-water mixture flows over erodible bed. *J. Hydr. Engrg.,* ASCE, 119(11), 1508-1525.

Table 1: Basic Data from the 1994 Experiments

Material	Run	Q_w	G_s	χ_f	Bed Type	h_n	S_n	c	$\Delta\eta$	L
		cm^3/s	g/s			cm		cm/s	cm	Cm
Quartz 19	1	78.8	0.98	0.0047	SS	0.30	0.0270	0.14	4.0	L
	2	62.1	1.33	0.0080	DMSH	0.38	0.0244	N	N	N
	3	50.9	1.75	0.0128	MS	0.27	0.0403	0.21	3.2	130
	4	37.5	2.22	0.0219	MS	0.32	0.0354	0.15	2.9	L
	5	32.3	2.64	0.0299	MS	0.20	0.0469	0.10	3.8	L
	6	26.3	3.20	0.0439	SS	0.27	0.0634	0.09	4.2	L
	7	24.2	4.61	0.0671	SS	0.30	0.1043	0.02	5.4	L
	8	16.6	5.86	0.1176	SS	0.22	0.0907	0.11	5.7	L
	9	11.7	7.02	0.1846	SS	0.18	0.0997	0.08	3.7	L
	10	86.6	1.24	0.0054	DMSH	0.52	0.0351	N	N	N
	11	74	1.81	0.0091	DMSH	0.43	0.0353	N	3.9	N
	12	70.6	2.33	0.0123	MS	0.38	0.0374	0.11	3.9	75
	13	50.5	2.70	0.0198	MS		0.0280	0.18	4.0	135
	14	38.2	3.33	0.0318	MS		0.0390	0.12	3.9	107
	15	26.1	5.16	0.0694	SS	0.20	0.0745	0.15	5.5	L
	16	41	0.53	0.0049	F	0.25	0.0366	0	0	0
	17	39.4	0.96	0.0091	SS	0.22	0.0469	0.1	3.9	L
	18	60	0.54	0.0034	F	0.28	0.0314	0	0	0
	19	41.2	0.87	0.0079	F	0.20	0.0406	0	0	0
	20	25.4	2.72	0.0388	SS	0.19	0.0445	0.10	N	L
	21	28.5	3.78	0.0477	SS	0.20	0.0447	0.16	4.1	L
	22	36	3.7	0.0373	MS	0.21	0.0455	0.13	4.1	99
	23	35.7	4.16	0.0421	MS	0.30	0.0610	0.14	2.6	64
	24	35.9	4.46	0.0448	MS	0.30	0.0480	0.26	3.4	63
	25	35.7	5.08	0.0510	MS	0.27	0.0539	0.15	5.0	57
	26	35.6	5.96	0.0594	MS	0.26	0.0598	0.13	3.2	74
	27	9.6	6.04	0.1919	SS	0.17	0.0941	0.07	2.0	L
	28	17.5	5.82	0.1115	SS	0.14	0.1020	0.11	5.3	L
	29	30.1	0.51	0.0064	F	0.22	0.0393	0	0	0
Silica 45	1	35.4	0.58	0.0061	F	0.27	0.0426	0	0	0
	2	21	0.56	0.0100	F	0.17	0.0506	0	0	0
	3	60	0.58	0.0036	DMSH	0.43	0.0185	N	N	N
	4	35.2	2.93	0.0305	MS	0.19	0.0459	0.24	2.4	95
	5	35.2	6.11	0.0615	MS	0.30	0.0590	0.40	3.1	65
	6	35	8.46	0.0836	MS	0.22	0.0509	0.33	3.0	79
	7	41.9	3.03	0.0266	MS	0.29	0.0390	0.31	2.0	102
	8	55.4	3.00	0.0200	MS			0.27	2.8	115
	9	87.4	3.03	0.0129	DMSH	0.70	0.0220	N	N	N
	10	10.2	6.06	0.1831	F	0.35	0.1311	0	0	0
	11	10.2	2.91	0.0972	SS	0.23	0.1180	0.06	1.9	L
	12	20.6	3.03	0.0526	MS	0.30	0.0860	0.21	2.2	124
	13	20.6	6.18	0.1017	MS	0.20	0.0880	0.27	3	120
	14	11	8.19	0.2193	F	0.46	0.1371	0	0	0
	15	53.6	3.11	0.0214	MS			0.30	3.2	116
	16	72.2	2.98	0.0153	MS			0.35	2.6	102
	17	35.8	1.83	0.0189	F	0.16	0.0526	0.25	3	0
	18	10.7	0.52	0.0180	SS	0.16	0.0670	0	N	L
Silica 120	1	10.3	0.64	0.0229	F	0.14	0.1030	0	0	0
	2	35.5	0.62	0.0065	F	0.24	0.0670	0	0	0
	3	47.9	0.61	0.0048	F	0.29	0.0590	0	0	0
	4	36.1	2.76	0.0280	SCP	0.18		0.16	2.0	55
	5	10.9	2.76	0.0872	F	0.12	0.1660	0	0	0

	6	10.7	1.72	0.0572	F	0.18	0.1385	0	0	0
	7	59.7	5.07	0.0311	MS	0.24		0.55	2.5	55
	8	45.7	4.06	0.0324	SCP	0.28		0.29	6.6	N
	9	71.4	6.7	0.0342	MS	0.30		0.90	3	66

Notes: F = flat, SS = single step, MS = multiple steps, SCP = chute-and-pool steps, DMSH = downstream-migrating scour holes, N = not measured, L = wavelength too long to measure.

Table 2: Calculated Dimensionless Parameters for the 1994 Experiments

Material	Run	$\mathbf{Re}_b$	τ_b^*	C_{fb}
Quartz 19	1	6119	2.43	0.0025
	2	4685	2.73	0.0076
	3	3915	3.28	0.0069
	4	2817	3.38	0.0188
	5	2590	2.87	0.0078
	6	1980	5.17	0.0423
	7	1685	9.38	0.1293
	8	1350	6.08	0.0727
	9	1045	5.52	0.0748
	10	6034	5.22	0.0153
	11	5417	4.43	0.0115
	12	5306	4.19	0.0090
	15	2127	4.56	0.0183
	16	3156	2.77	0.0077
	17	3073	3.15	0.0073
	18	4627	2.65	0.0043
	19	3259	2.49	0.0042
	20	2057	2.59	0.0101
	21	2324	2.74	0.0092
	22	2905	2.92	0.0069
	23	2695	5.49	0.0296
	24	2756	4.32	0.0222
	25	2809	4.39	0.0179
	26	2836	4.70	0.0175
	27	873	4.93	0.0858
	28	1537	4.43	0.0171
	29	2333	2.64	0.0105
Silica 45	1	2674	1.465	0.0156
	2	1655	1.119	0.0128
	3	4432	0.979	0.0090
	4	2846	1.130	0.0054
	5	2719	2.241	0.0281
	6	2939	1.442	0.0086
	7	3241	1.435	0.0119
	9	5486	1.784	0.0250
	11	700	3.487	0.3988
	12	1390	3.266	0.1566
	13	1697	2.276	0.0340
	17	2885	1.097	0.0037
	18	829	1.398	0.0569
Silica 120	1	805	0.708	0.0629
	2	2694	0.773	0.0173
	3	3594	0.814	0.0146
	5	922	0.982	0.0493
	6	765	1.214	0.1938

Note: runs for which depth was not measured are omitted from the table. A few runs were omitted because the removal of wall effects yielded unrealistic results.

Table 3: Characteristic Parameters of the Sediment

Sediment	D	v_s	$\mathbf{Re}_p$	C_{fa}	u_t	ω	τ_{th}^*	α_t (n = 1.5)	α_t (n = 1.8)	α_t (n = 2.0)
	mμ	cm/s			cm/s					
Quartz 19	19	0.032	0.333	0.0117	10.13	0.0032	0.389	0.00315	0.00247	0.00169
Silica 45	45	0.180	1.21	0.0134	8.23	0.0219	0.125	0.0137	0.0130	0.0130
Silica 120	120	1.010	5.29	0.0160	10.59	0.0954	0.092	0.0101	0.0104	0.0104

Table 4: Dimensionless Parameters Associated with Step Formation for the 1994 Experiments

Material	Run	S_t	$\mathbf{Fr}_t$	$\mathbf{Fn}_t$	$\hat{c}$	$\Delta\hat{\eta}$	$\hat{L}$
Quartz 19	1	0.00078	0.259	3.077	1.775	2.559	
	3	0.00120	0.321	2.347	0.971	3.144	0.153
	4	0.00161	0.372	1.352	0.407	3.832	
	5	0.00186	0.399	2.377	0.198	5.781	
	6	0.00225	0.439	1.252	0.121	7.734	
	7	0.00238	0.452	1.008	0.018	10.545	
	8	0.00329	0.531	1.164	0.055	15.348	
	9	0.00431	0.608	1.200	0.026	13.061	
	12	0.00086	0.272	1.948	0.530	2.764	0.046
	13	0.00120	0.321		0.539	3.933	0.159
	14	0.00157	0.366		0.223	5.007	0.215
	15	0.00220	0.435	2.002	0.128	9.933	
	17	0.00155	0.365	2.461	0.650	4.968	
	20	0.00234	0.448	2.038	0.152		
	21	0.00207	0.421	2.137	0.199	6.940	
	22	0.00165	0.376	2.481	0.206	5.553	0.222
	23	0.00166	0.377	1.448	0.197	3.534	0.144
	24	0.00164	0.375	1.461	0.344	4.582	0.140
	25	0.00164	0.375	1.712	0.174	6.733	0.126
	26	0.00163	0.374	1.823	0.130	4.283	0.162
	27	0.00520	0.668	1.082	0.022	8.528	
	28	0.00314	0.519	2.401	0.058	13.630	
Silica 45	4	0.00105	0.280	2.799	0.575	2.720	0.113
	5	0.00102	0.275	1.458	0.474	3.401	0.072
	6	0.00100	0.273	2.363	0.288	3.232	0.085
	7	0.00088	0.257	1.760	0.851	1.912	0.086
	8	0.00067	0.224		0.983	2.038	0.056
	11	0.00337	0.501	0.654	0.045	6.919	
	12	0.00175	0.361	0.845	0.291	4.163	0.411
	13	0.00166	0.352	1.637	0.194	5.383	0.358
	15	0.00070	0.228		1.021	2.404	0.061
	16	0.00052	0.197		1.664	1.459	0.030
Silica 120	7	0.00157	0.313	3.346	1.004	2.148	0.074
	9	0.00130	0.286	2.873	1.492	2.148	0.062

Note: only runs with steps are included above.

Table 5: Detailed Parameters for Selected Runs from 1994 and 1997

Year	Material	Run	Q_w	G_s	S_n	S_e	h_n	h_e	c	$\Delta\eta$	L	θ_{max}
			cm^3/s	g/s			cm	cm	cm/s	cm	cm	Deg
1994	Quartz 19	23	35.7	4.16	0.061	0.0505	0.3		0.14	2.31	48	15-29
1994	Silica 45	6	35.0	8.46	0.0509	0.0617	0.22		0.33	2.21	70	23-47
1994	Silica 120	7	59.7	5.07		0.0655			0.55	2.55	49	17-25
1994	Silica 120	9	71.4	6.7		0.0723			0.90	3.48	65	21-31
1997	Silica 45	6	55.4	3.95		0.0430		0.335	0.36	2.77	113	
1997	Silica 45	7	55.3	5.07		0.0485		0.315	0.26	2.36	106	

Note: the values of $\Delta\eta$ and L in the above table are not identical to the values given in Table 1 because they were measured in a different way.

FIGURE CAPTIONS

Figure 1. View from Run 6 of the 1997 series showing three complete steps and part of a fourth step. The sediment is Silica 45. Flow is from left to right.

Figure 2. View from Run 7 of the 1994 series using Silica 120. Two steps, each terminating in a hydraulic jump, are clearly visible. Flow is from left to right.

Figure 3. a) View of a step from Run 11 of the 1994 series using Quartz 19. Flow is from left to right.
b) View of the same step a short time later, illustrating upstream migration. Flow is from left to right.

Figure 4. View of the experimental apparatus.

Figure 5. Definition diagram showing step wavelength L, migration speed c, equilibrium slope S_e in the presence of steps and wave height $\Delta\eta$.

Figure 6. Illustration of the mode of bed aggradation before the formation of steps.

Figure 7. View of the bed profile prevailing before the onset of cyclic steps. Flow is from left to right.

Figure 8. Steps formed in Run 24 of the 1994 experiments using the Quartz 19 material. Flow is from left to right.

Figure 9. Plot of bed resistance coefficient C_{fb} versus h_n/D for the data pertaining to verifiably turbulent flow.

Figure 10. Plot of the empirically determined values of critical Shields stress τ_{th}^* at the threshold of motion and coefficients α_t in the sediment entrainment relation as functions of particle Reynolds number $\mathbf{Re}_p$. Values of α_t are shown for each of the exponents n = 1.5, 1.8 and 2.0. Also shown is the curve for τ_{th}^* versus $\mathbf{Re}_p$ due to Mantz (1982).

Figure 11. Plot of the ratio E/α_t versus $\tau_b^* - \tau_{th}^*$ for the data pertaining to verifiably turbulent flow, as well as the regression relation determined from the data, for
a) n = 1.5;
b) n = 1.8; and
c) n = 2.0.

Figure 12. a) Plot of bed type as a function of $\mathbf{Fr}_t$ and $\mathbf{Fr}_n$ for the 19 micron material.
b) Plot of bed type as a function of $\mathbf{Fr}_t$ and $\mathbf{Fr}_n$ for the 45 micron material.
c) Plot of bed type as a function of $\mathbf{Fr}_t$ and $\mathbf{Fr}_n$ for the 120 micron material.

Figure 13. a) Plot of dimensionless wave speed $\hat{c}$ as a function of $\mathbf{Fr}_t$ and $\mathbf{Fr}_n$ for the 19 micron material.
b) Plot of dimensionless wave speed $\hat{c}$ as a function of $\mathbf{Fr}_t$ and $\mathbf{Fr}_n$ for the 45 micron material.

Figure 14. a) Plot of dimensionless wave height $\Delta\hat{\eta}$ as a function of $\mathbf{Fr}_t$ and $\mathbf{Fr}_n$ for the 19 micron material.

b) Plot of dimensionless wave height $\Delta\hat{\eta}$ as a function of $\mathbf{Fr}_t$ and $\mathbf{Fr}_n$ for the 45 micron material.

Figure 15. a) Plot of dimensionless wavelength $\hat{L}$ as a function of $\mathbf{Fr}_t$ and $\mathbf{Fr}_n$ for the 19 micron material.

b) Plot of dimensionless wavelength $\hat{L}$ as a function of $\mathbf{Fr}_t$ and $\mathbf{Fr}_n$ for the 45 micron material.

Figure 16. a) Image of a downstream-migrating scour hole from Run 11, Quartz 19 material, 1994.

b) View of the same downstream-migrating scour hole a short time later.

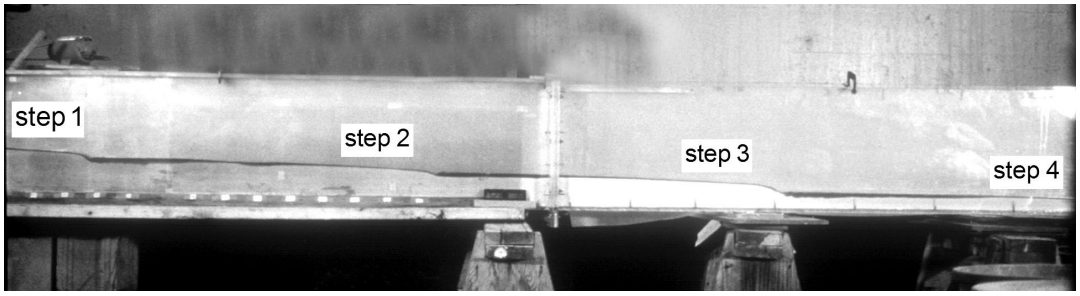

Figure 1.

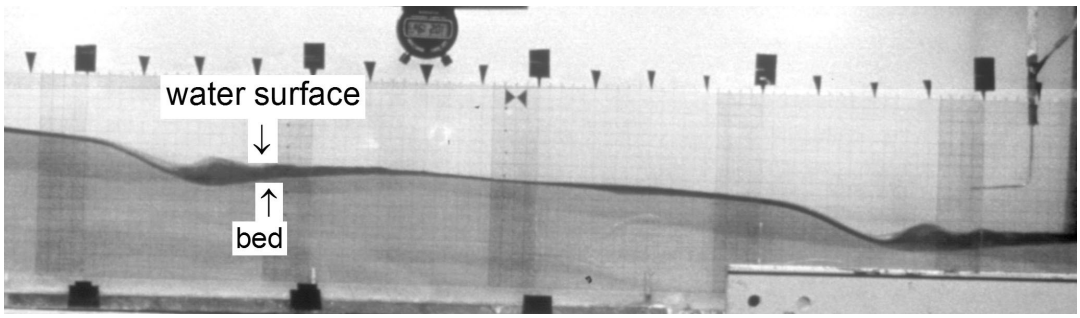

Figure 2

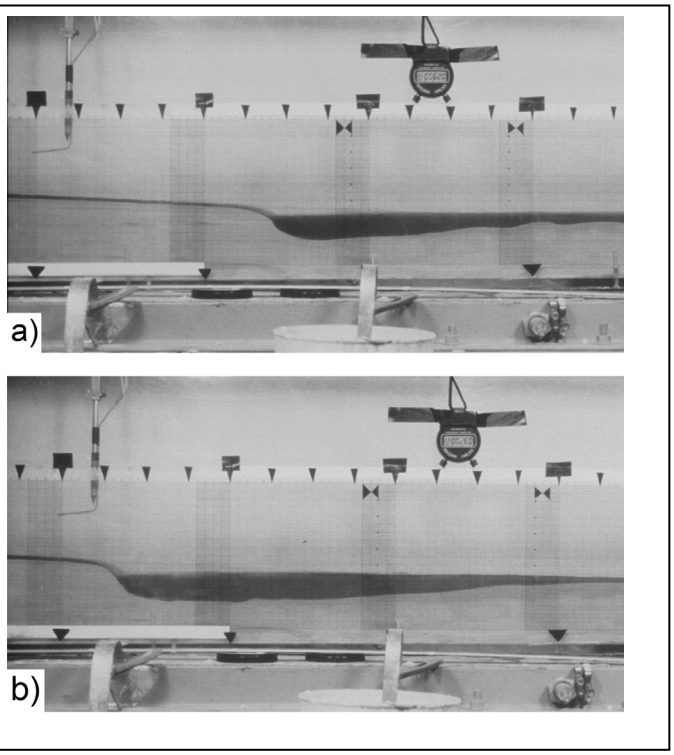

Fig. 3a,b

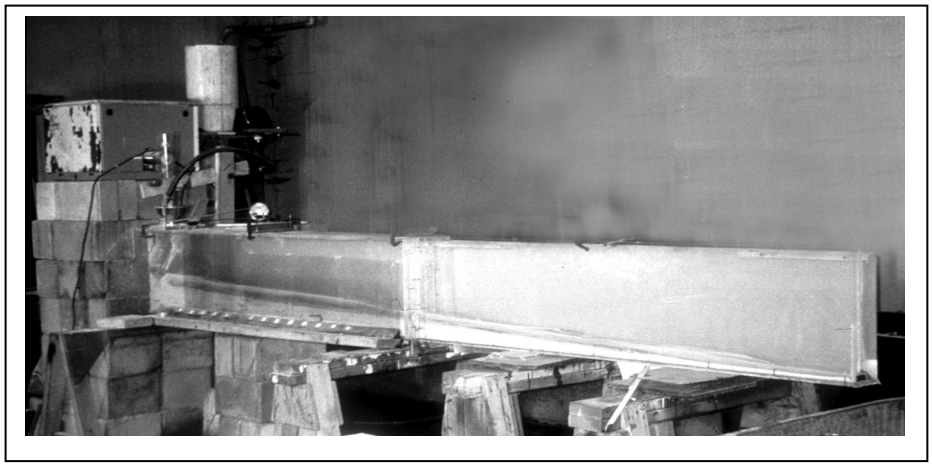

Fig. 4

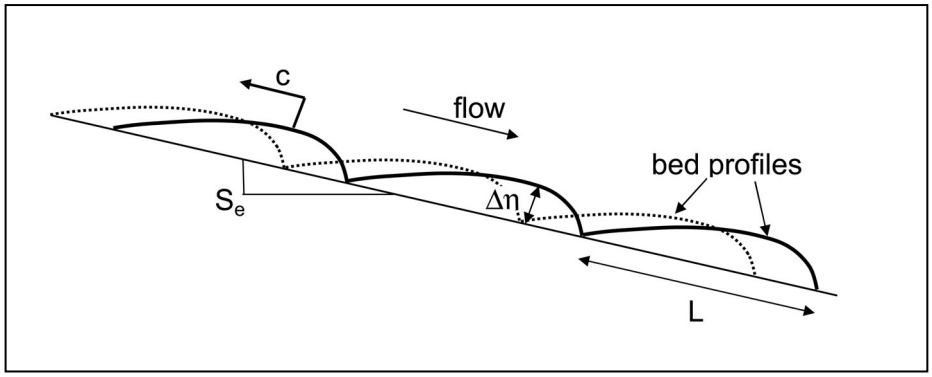

Fig. 5

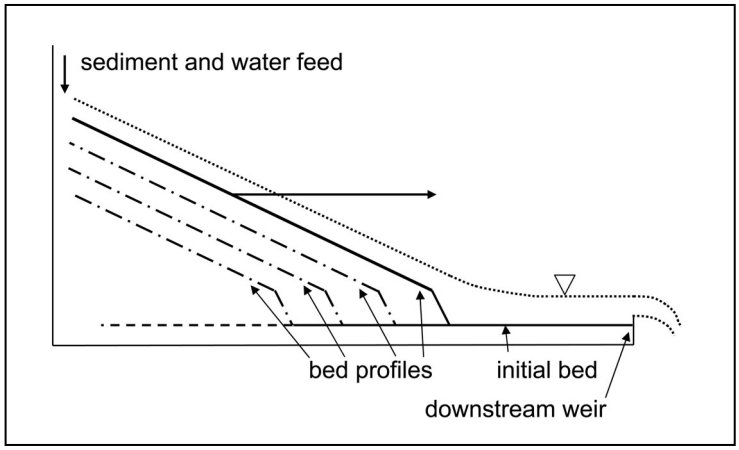

Fig. 6

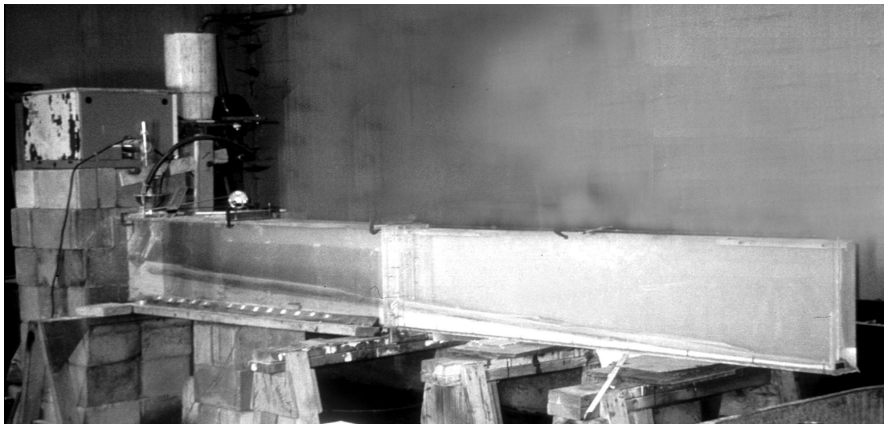

Fig. 7

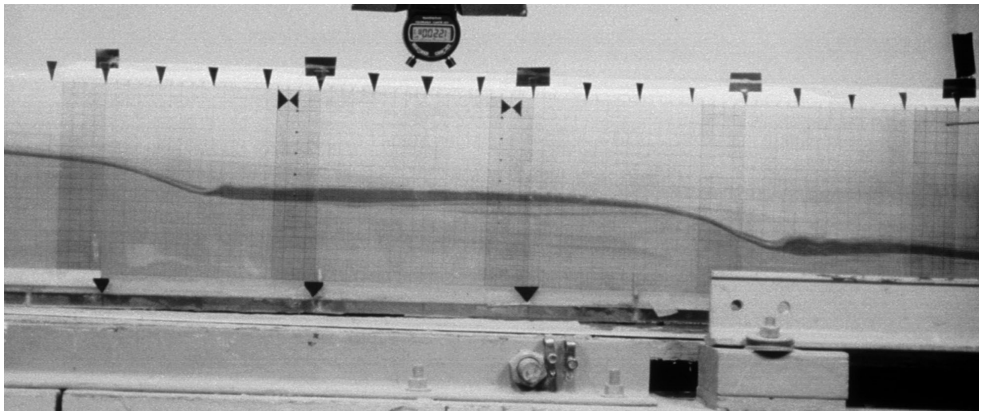

Fig. 8

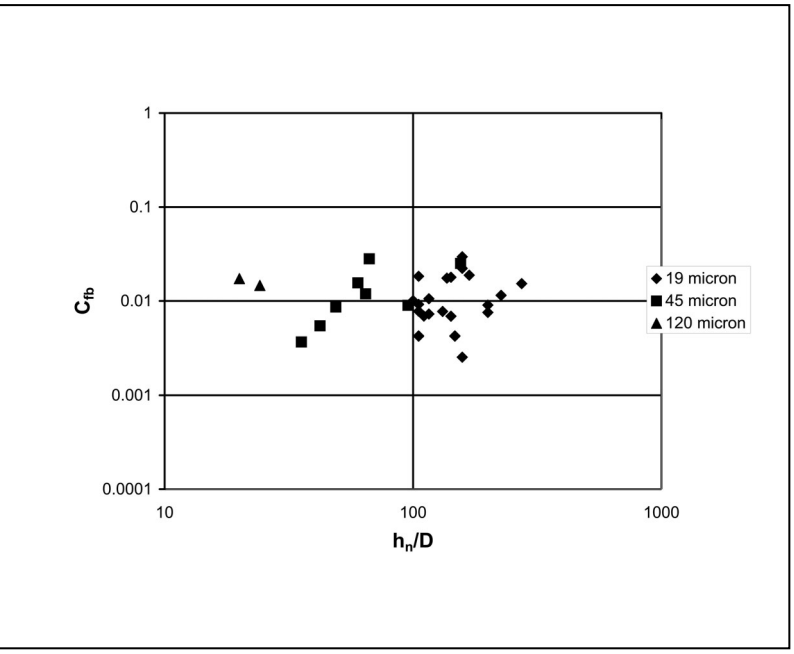

Fig. 9

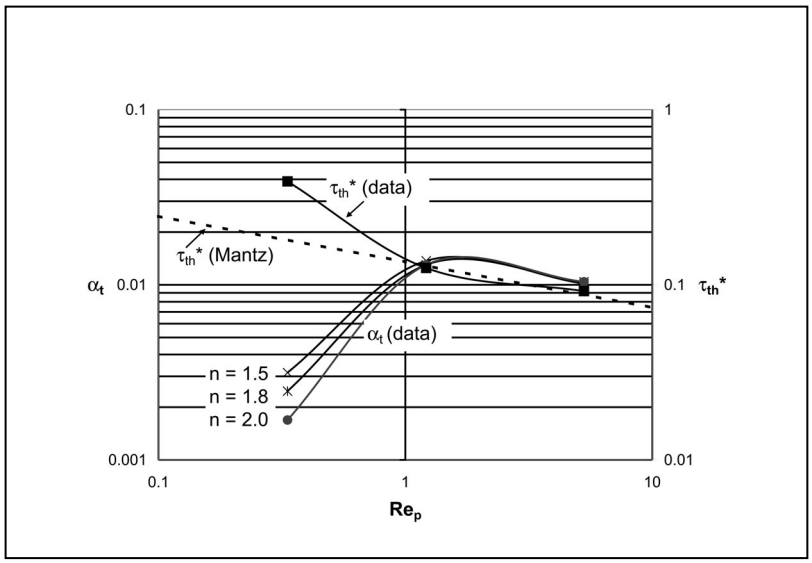

Fig. 10

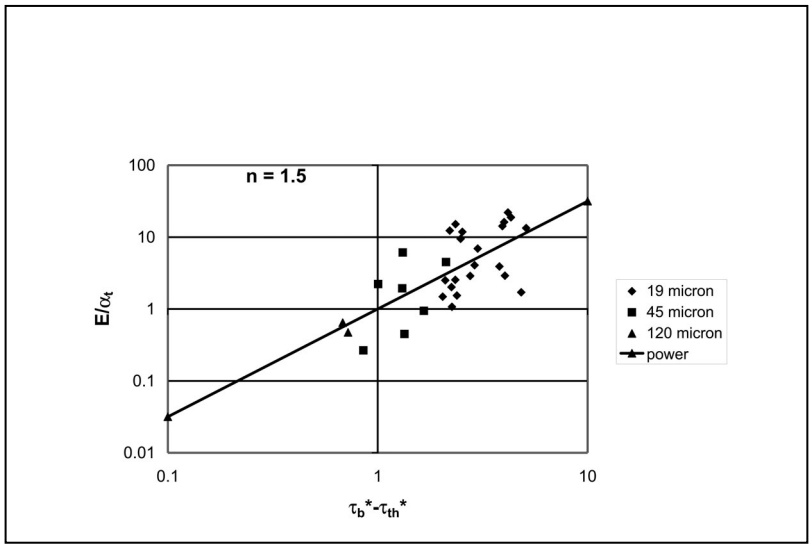

Fig. 11a

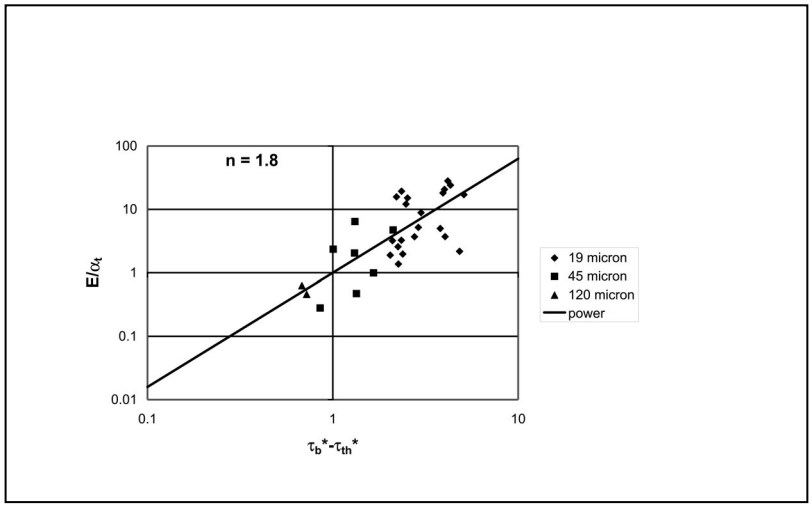

Fig. 11b

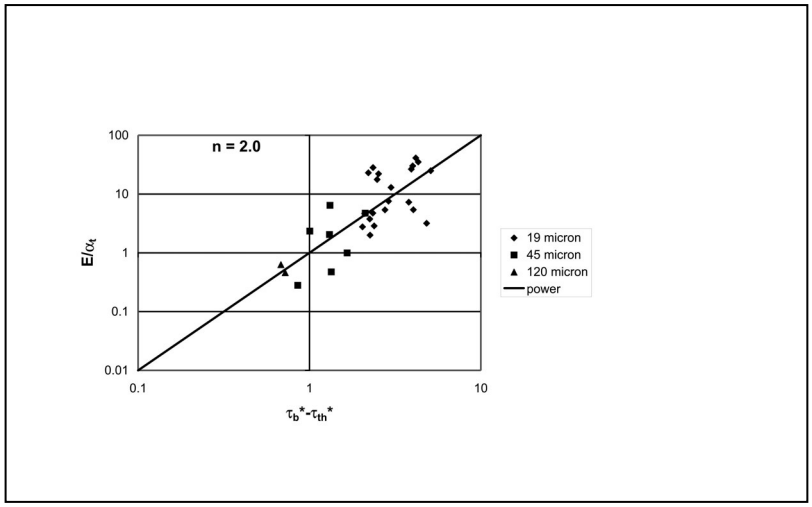

Fig. 11c

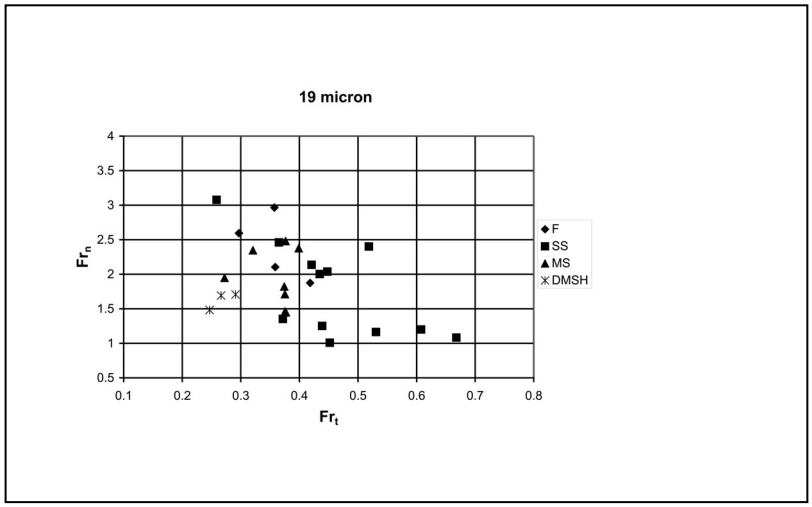

Fig. 12a

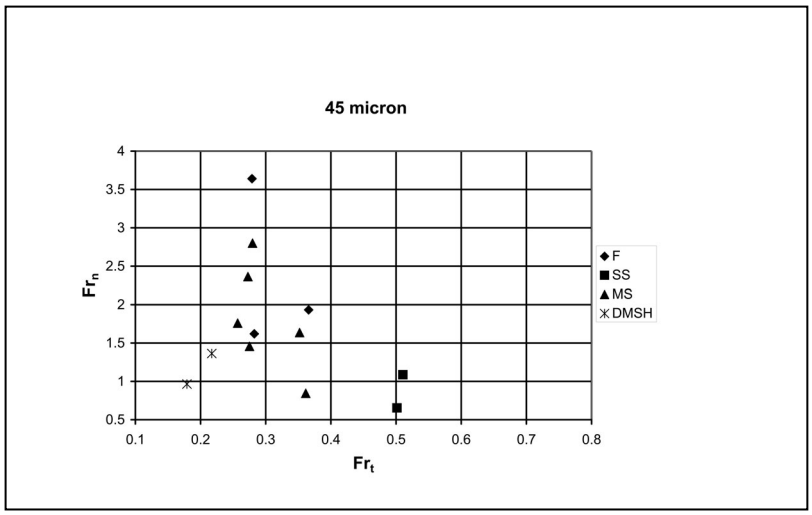

Fig. 12b

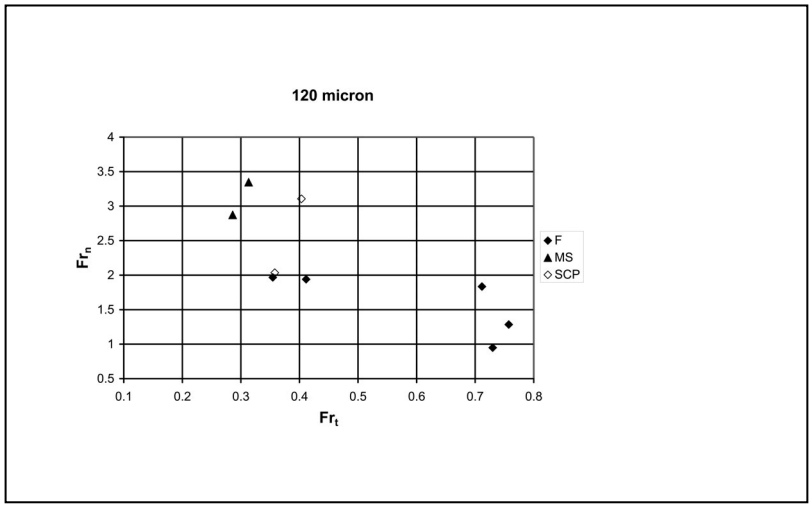

Fig. 12c

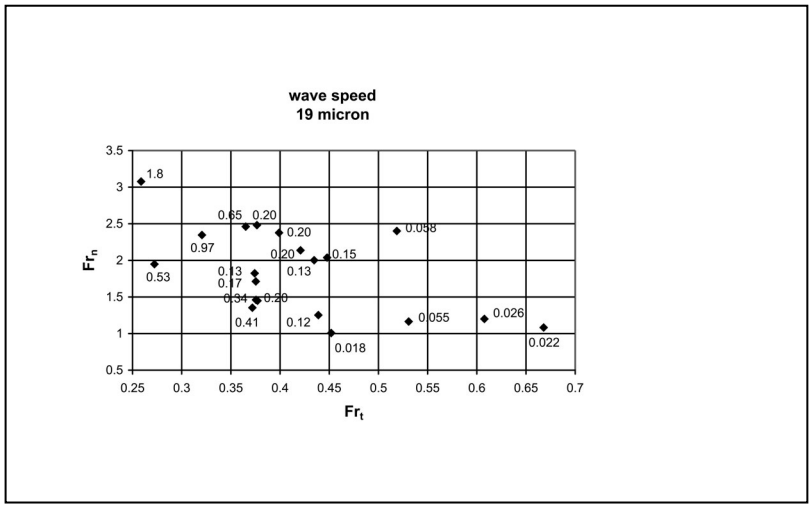

Fig. 13a

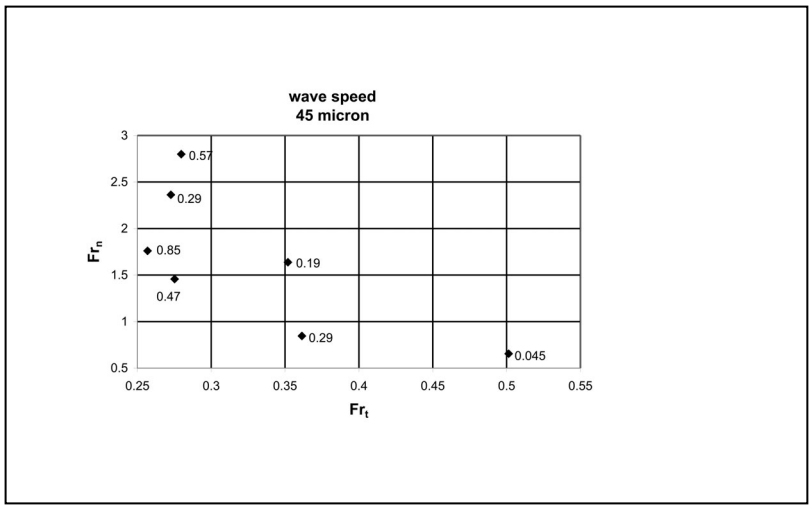

Fig. 13b

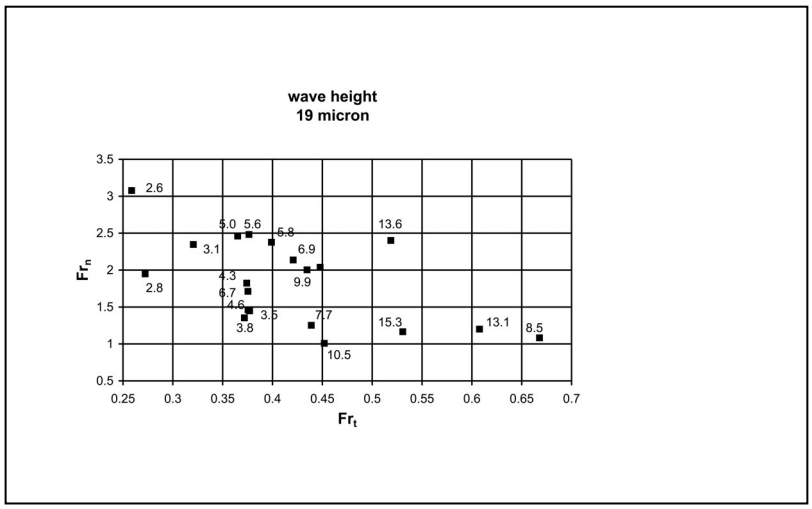

Fig. 14a

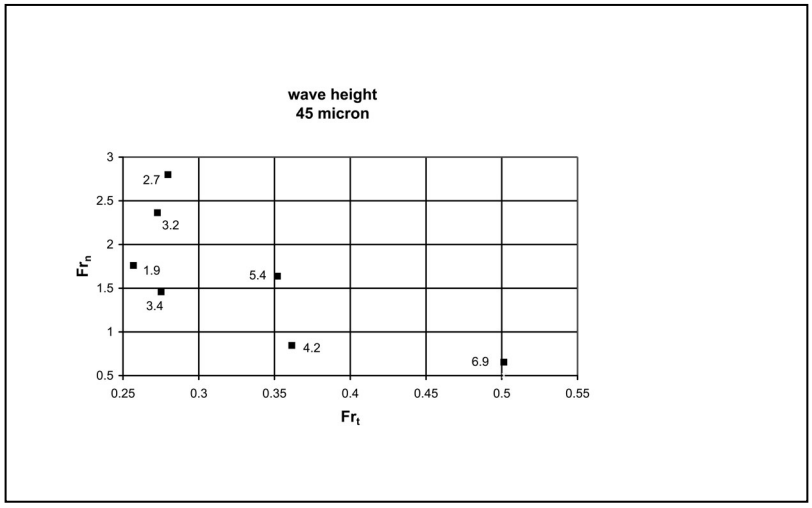

Fig. 14b

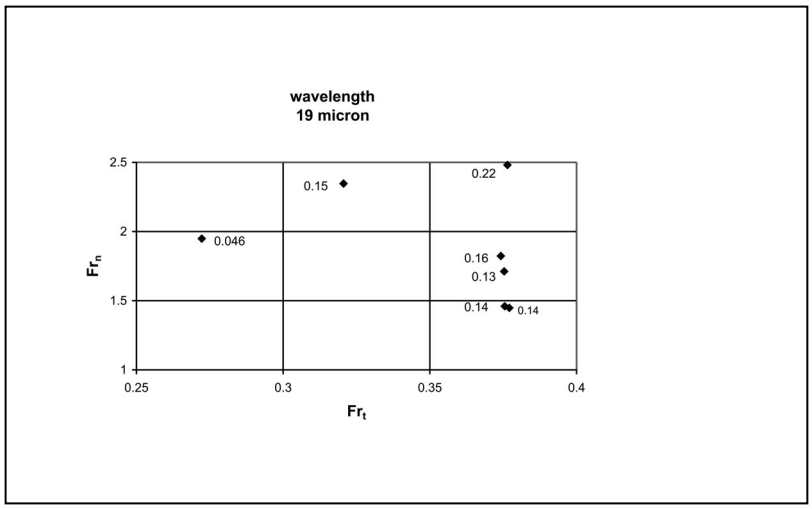

Fig. 15a

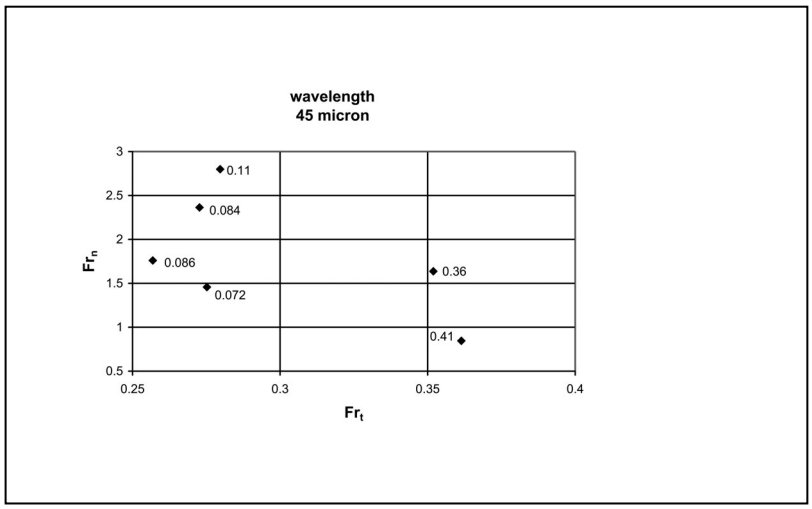

Fig. 15b

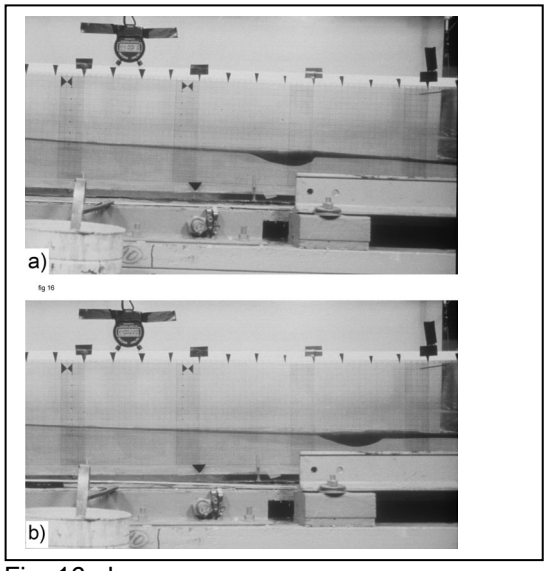

Fig. 16a,b